

www.acsaem.org Article

# Impact of Triethyl Borate on the Performance of 5 V Spinel/Graphite Lithium-Ion Batteries

Tianyang Wang, Lalith Rao, Xinwei Jiao, Junbin Choi, Junwei Yap, and Jung-Hyun Kim\*



Cite This: ACS Appl. Energy Mater. 2022, 5, 7346-7355



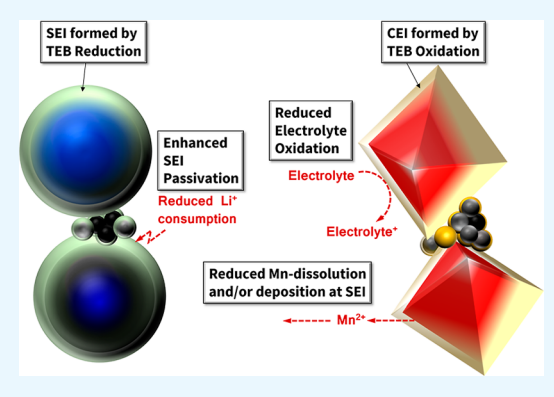
**ACCESS** 

Metrics & More

Article Recommendations

s Supporting Information

ABSTRACT: Positive roles of triethyl borate (TEB) electrolyte additive on high-voltage lithium-ion batteries were investigated in Li-Ni<sub>0.5</sub>Mn<sub>1.5</sub>O<sub>4</sub>(LNMO)/graphite full-cells. A capacity fading of the LNMO/graphite full-cells originates from the Mn dissolution of LNMO cathodes and a degradation of graphite SEI, which unwantedly consumes active Li<sup>+</sup>. Because the Li<sup>+</sup> loss cannot be measured in a half-cell configuration (i.e., LNMO/Li), we designed a systematic experiment to understand the effect of TEB on the electrode–electrolyte interphases in the full-cells: cathode–electrolyte interphase (CEI) of LiNi<sub>0.5</sub>Mn<sub>1.5</sub>O<sub>4</sub> (LNMO) and solid–electrolyte interphase (SEI) of graphite, respectively. Among various TEB contents (0–4 wt %) investigated, 1 wt % TEB offered combined advantages of high specific capacity and low full-cell impedance during extended cycling. The TEB contributed to the production of a CEI layer and suppressed Mn



dissolution on LNMO cathode during long-term cycling. A combinatorial study of TEB-treated graphite and TEB-treated LNMO electrodes, however, suggested that an early-stage performance improvement shown by the full-cells was mostly contributed by an improved SEI stability on graphite anodes and a reduced Li<sup>+</sup> loss, as evidenced by X-ray photoelectron spectroscopy data. Although literature data mostly focused on the impacts of TEB on CEI in half-cell configurations, our full-cell analyses revealed an additional benefit of TEB in significant improving stability of graphite SEI. Our results suggest that TEB can contribute to CEI and SEI simultaneously, which can offer promising performance improvements in various types of high-voltage LIBs.

**KEYWORDS:** triethyl borate, electrolyte additive, high-voltage Li-ion batteries, cathode electrolyte interphase (CEI), solid-electrolyte interphase (SEI)

### **■ INTRODUCTION**

Lithium-ion batteries (LIBs) have been widely adopted for power sources in large-scale applications because of the high energy density and long cycle life. Lespecially, the recent growth of electric vehicle (EV) market requires further improvement in the performance of LIBs. In the past decade, many researchers have considered high-voltage spinel Li-Ni<sub>0.5</sub>Mn<sub>1.5</sub>O<sub>4</sub> (LNMO) as the next generation cathode material because of its high operating voltage (~4.7 V vs Li/Li<sup>+</sup>) and high energy density. Furthermore, its good rate capability stemming from 3-dimensional Li<sup>+</sup> diffusion pathway in a crystal lattice and cobalt-free chemical composition offer significant benefits such as fast-charging capability, reduced cost, and environment friendliness. A

Nevertheless, the main challenge of the LNMO commercialization is also caused by the high operating voltage that exceeds the electrolyte stability window. The most commonly used electrolyte formula are mixtures of lithium hexafluorophosphate (LiPF $_6$ ) salt and organic carbonate solvents. The high operating potential of LNMO beyond the stability limit of carbonate-based electrolytes ( $\sim$ 4.3 V vs Li/Li $^+$ ) results in an oxidative decomposition of the conventional electrolytes. The

electrolyte oxidation also produces HF that can trigger the Mn-dissolution issue, which originates from a disproportionation reaction of  $\mathrm{Mn^{3^+}}$  into  $\mathrm{Mn^{4^+}}$  and  $\mathrm{Mn^{2^+}}.^{12}$  The Mn in LNMO is dissolved and migrates to anode side, followed by attacking the solid electrolyte interphase (SEI) layer on anodes. The damaged SEI is recovered subsequently by consuming  $\mathrm{Li^+}$  and electrolyte, which unwantedly reduces residual capacity of LIB cells. Because the Mn dissolution occurs continuously during cycling, such  $\mathrm{Li^+}$  loss from LNMO cathode is known to be the major degradation mechanism of the LNMO/graphite full-cells.

Intensive R&D effort has been made to improve electrolyte and electrode—electrolyte interphase stabilities in high-voltage cells. The most effective and economical pathway has been to employ electrolyte additives into baseline electrolytes. <sup>14</sup> The

 Received:
 March 20, 2022

 Accepted:
 May 16, 2022

 Published:
 May 26, 2022





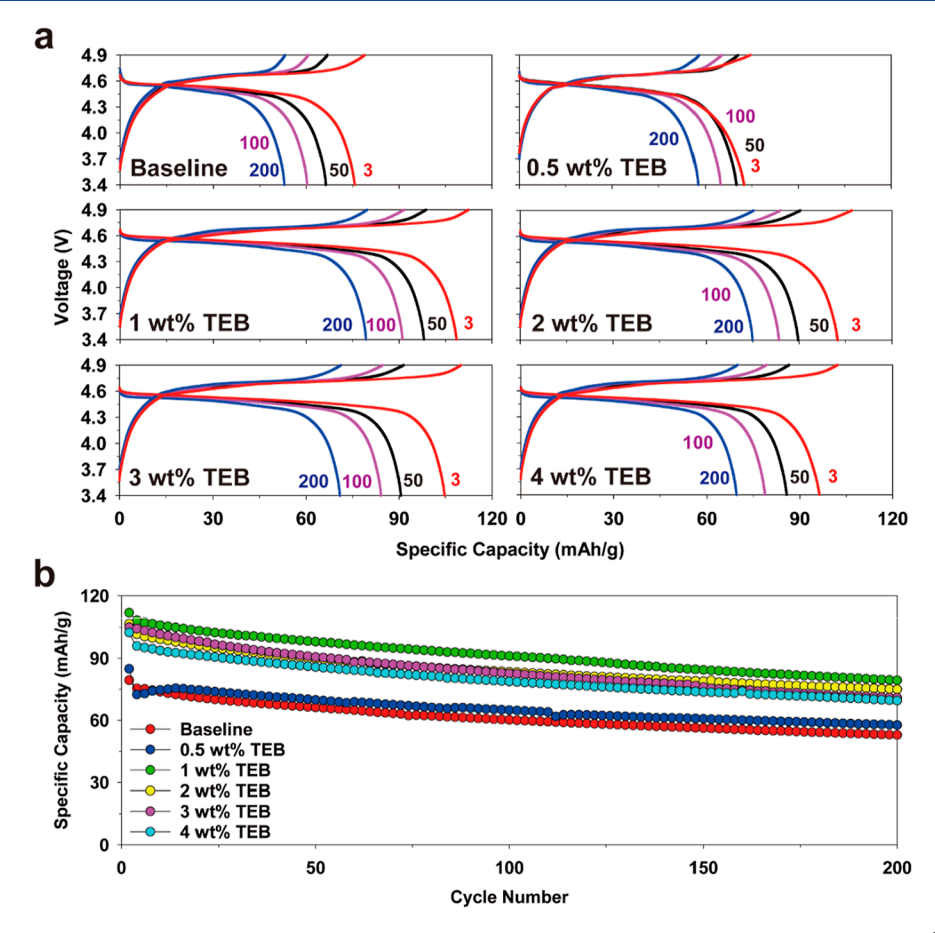


Figure 1. (a) Voltage profiles of LNMO/graphite full-cells with baseline, 0.5, 1, 2, 3, and 4 wt % TEB additives in electrolytes; (b) cycling performance of LNMO/graphite full-cells at 25 °C. First two cycles were performed at C/10 rate, followed by C/3 rate cycling during the rest.

additives can be preferentially oxidized at CEI or reduced at SEI and can produce artificial passivation layers, which are often more robust and stable compared with those layers from the baseline electrolyte. 15,16 Such improved passivation layers can suppress parasitic reactions occurring at CEI and/or SEI and consequently reduce active Li<sup>+</sup> consumption during LIB cycling. Among various additives, borate compounds such as lithium bis(oxalate) borate (LiBOB),<sup>17</sup> triethyl borate (TEB),<sup>18</sup> and trimethyl borate (TMB)<sup>19</sup> showed promising capability of stabilizing the electrode-electrolyte interphases and improving the cell performances. In particular, the TEB additive offered performance improvement of high-voltage cathodes such as  $\text{Li}[\text{Li}_{0.2}\text{Ni}_{0.13}\text{Mn}_{0.54}\text{Co}_{0.13}]\text{O}_2$ ,  $\text{LiNi}_{1/3}\text{Mn}_{1/3}\text{Co}_{1/3}\text{O}_2$ , and LNMO in half-cells (using Li metal as anodes).  $^{18,20,21}$  It was reported that the main benefits of TEB were improving cycle life and rate capability and suppressing structural transformation of cathode active materials. <sup>20,22</sup> In particular, TEB additive could improve the performance of LNMO/Li half-cell by forming a thin and protective CEI layer on LNMO cathodes and suppressing the oxidative decomposition of electrolytes.<sup>21</sup>

However, there is a lack of literature data providing the performance evaluation and characterization of TEB additives in full-cells (using graphite anodes), which are real-world LIB configuration. Unlike metallic anodes in half-cells, the high-voltage LIB performances have been governed by the SEI stability on graphite due to the complex reaction mechanisms in full-cells associated with the migration of byproducts from cathode to anode SEI. Given the fact that the parasitic reactions at CEI and SEI are closely associated with each other, such as the

Mn-dissolution issue, it is important to understand the effect of TEB at the full-cell level. More importantly, performance degradation and the resulting Li<sup>+</sup> loss from LNMO cathode can be distinguishable only from the full-cell configuration; in contrast, half-cells have unlimited Li<sup>+</sup> supply from the metallic Li anodes and conceals the Li<sup>+</sup> loss in the cells. <sup>13</sup> In this regard, we systematically designed an experiment to examine the effect of TEB additive on the LNMO/graphite full-cell performances. The results were combined with analytical data of full-cells via spectroscopies and scanning electron microscopy (SEM) to understand the TEB's effect on CEI and SEI layers.

#### EXPERIMENTAL SECTION

Preparation of Electrodes and Electrolyte. LNMO (MTI Corporation) was used as received. Cathode consisted of 85 wt % LNMO, 7.5 wt % Super-P, and 7.5 wt % polyvinylidene fluoride (PVdF) binder. For anodes, metallic lithium (Li) (Alfa Aesar) and mesocarbon microbeads (MCMB, MTI Corporation) graphite were used, respectively, in half- and full-cells. The graphite anodes consisted of 80 wt % graphite, 10 wt % Super-P, and 10 wt % PVdF binder. Both cathode and anode materials were mixed in an N-methyl-2-pyrrolidone (NMP) solvent to form a slurry. The obtained slurry was coated on an aluminum foil for cathodes and copper foil for anodes by using a doctor blade. The electrodes were dried at 80 °C in an oven for 1 h, followed by calendering process and vacuum drying at 100 °C (for cathodes) or 80 °C (for anodes) for 24 h. The baseline electrolyte formula was 1 M  $LiPF_6$  in ethylene carbonate (EC)/ethyl methyl carbonate (EMC) = 1:1 w/w (Gotion). TEB (Sigma-Aldrich, 99% purity) was used as received. Various amounts of TEB additive (0.5, 1, 2, 3, and 4 wt %) were dissolved in the baseline electrolyte in an argon-filled glovebox overnight.

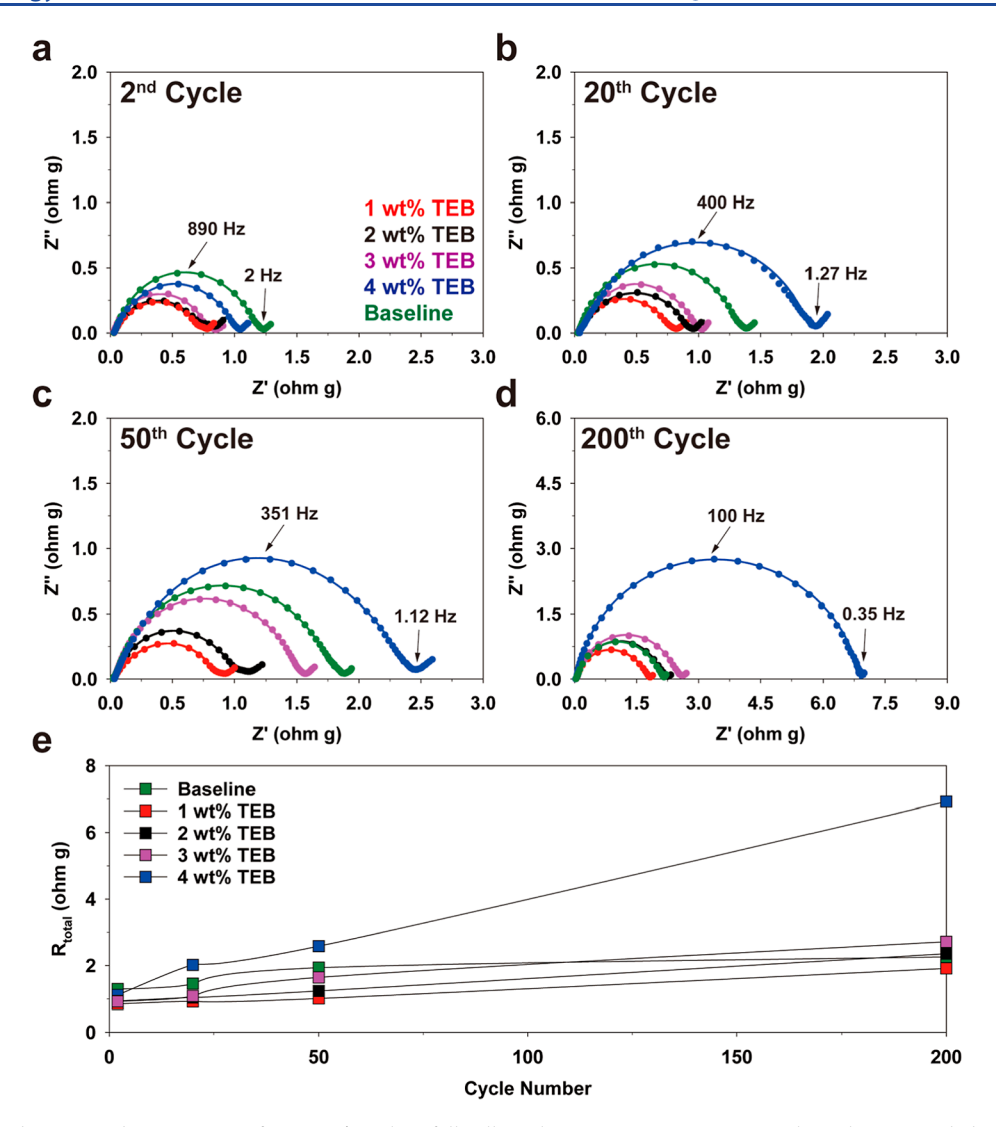


**Figure 2.** Normalized AC-impedance spectra of LNMO/graphite full-cells with various TEB contents in electrolytes recorded at (a) 2nd cycle, (b) 20th cycle, (c) 50th cycle, and (d) 200th cycle at 25 °C. (e) Evolution of total polarization resistances ( $R_{\text{total}} = R_{\text{ohmic}} + R_{\text{int}} + R_{\text{CT}}$ ) of the full-cells with cycle numbers.

**Electrochemical and Physical Characterization.** Coin half- and full-cells (CR2032) were assembled inside the argon-filled glovebox by applying a piece of polypropylene separator (Celgard 2500) and 100  $\mu$ L electrolyte. All the cells were tested using battery-testing stations (Arbin LBT) at 25 °C in an environmental chamber. The potential range for full-cell galvanostatic testing was 3.4–4.9 V. The cells were cycled twice at C/10 rate at the beginning (formation cycles), followed by C/3 rate during the rest period of the cycling. Electrochemical impedance spectroscopy (EIS) was measured using a potentiostat (Gamry Interface 1010E), and the resulting spectra were fitted with ZView (Scribner Inc.) and Fityk software.

The Mn deposition amount on cycle-aged graphite anodes were examined by inductively coupled plasma—mass spectrometry (ICP—MS, PerkinElmer Sciex ELAN 6000) characterization. The anodes were recovered from LNMO/graphite full-cells after 200 cycles and were gently rinsed using dimethyl carbonate (DMC) to remove residual electrolyte salts (e.g., LiPF<sub>6</sub>). The graphite anode was digested in 25 mL aqua regia (HCl/HNO<sub>3</sub> = 3:1, v/v) and filtered to remove carbon residues before the ICP—MS characterization. Fourier-transform infrared (FTIR) spectroscopy (Thermo Nicolet 6700) was conducted with pristine and cycled electrode samples (electrode/KBr = 1:100 wt ratio) under nitrogen purging. Scanning electron microscopy (SEM, FEI APREO II) images of the pristine and 200 cycled electrodes in full-cells were acquired. The CEI composition of cycled LNMO cathodes

and SEI composition of cycled graphite anodes were also characterized by X-ray photoelectron spectroscopy (XPS, Kratos Axis Ultra XPS). All the aged electrodes in this study were collected from LNMO/graphite full-cells in a fully discharged state and gently rinsed by soaking electrodes in DMC for 2 min 2 times before use.

#### RESULTS AND DISCUSSION

Effect of TEB Additive on Full-Cell Performances. It has been reported that TEB additive had a beneficial impact on the cycle life of LNMO/Li half-cells. <sup>21</sup> For example, compared with the baseline electrolyte having 23.4% capacity retention, adding TEB in electrolyte in the range of 0.5–4 wt % led to the capacity retentions in the range of 40.1–72.6%. <sup>21</sup> Theoretical calculation using density functional theory (DFT) method indicated that TEB could readily oxidize at high voltages. In addition, undesirable catalytic reaction between LNMO and TEB can accompany the oxidation of conventional, carbonate-based electrolytes. Our earlier studies, however, revealed that the major performance degradation of LNMO cathode is not detectable in the half-cell configuration (i.e., using Li-metal anodes). <sup>7,12,13</sup> Instead, only full-cells (i.e., using graphite anodes), the real-world battery configuration, can properly

characterize the electrochemical degradation of the LNMO cathode. The major degradation mechanism of LNMO full-cells is associated with a Li-ion loss due to a degradation of graphite SEI from the Mn-dissolution problem from the LNMO cathode, which was discussed in detail in the earlier section.

Figure 1 compares the voltage profiles and cycle lives of LNMO/graphite full-cells with different amounts of TEB contents. The N/P ratios of all cells were 1.05. The full-cell with the baseline electrolyte (i.e., TEB-free electrolyte) delivered 82 mA h/g of initial discharge capacity at C/10 rate, which corresponds to ~40 mA h/g capacity fade compared with its half-cell capacity (see Figure 1a). The same degree of capacity loss was still observed from the full-cell with 0.5 wt % TEB. In contrast, full-cells with 1-4 wt % TEB contents delivered much higher initial capacities in the following order: 110 mA h/g for 1 wt % TEB, 106 mA h/g for 2 wt % TEB, 104 mA h/g for 3 wt % TEB, and 102 mA h/g for 4 wt % TEB. The full-cell with 1 wt % TEB retained 84.8% (at 100th cycle) and 73.34% (at 200th cycle) of initial C/3 rate capacity (at 3rd cycle). Under the same conditions, the baseline full-cell delivered 79.4% (at 100th cycle) and 69.7% (at 200th cycle). Among the series of the TEB contents in the range of 0-4 wt %, the 1 wt % TEB electrolyte provided the highest specific capacity during the continuous cycling of the full-cell. Although it was not clearly visible in fullcells, oxidative decomposition of TEB at ~3.81 V vs Li could be observed from LNMO/Li half-cells, as shown in Figure S1, which agrees well with the literature. 22 Also, dQ/dV profiles of graphite/Li half-cells (see, Figure S2) showed that reductive decomposition of TEB occurred at ~ 0.76 V vs Li, prior to EC reduction at  $\sim$ 0.7 V vs Li.  $^{9,23,24}$ 

Figure 2 shows the normalized AC-impedance spectra of each full-cell that were measured at 2nd, 20th, 50th, and 200th cycles after charging to 4.6 V at 25 °C. The Nyquist plots were fitted based on an electrical circuit model consisting of two resistance (R)-constant phase element (CPE) parallel components connected in series, followed by Warburg-type diffusion: R<sub>ohmic</sub>  $-[R_{int}/CPE_{int}] - [R_{CT}/CPE_{CT}] - W_{diff}$ . Here,  $[R_{int}/CPE_{int}]$  in a high-frequency region is assigned to the interfacial impedance of electrode-electrolyte interfaces and  $[R_{CT}/CPE_{CT}]$  in the midto-low frequency region is assigned to the charge-transfer (CT) process.<sup>25</sup> All the cells show a trend of increasing impedance with cycle number. However, their rates of impedance growth are significantly different. Table S1 lists the fitted values of electrolyte Ohmic resistances, interfacial impedances, and CT impedances of the full-cells. In general, all the full-cells show a trend of increasing electrolyte impedance ( $R_{Ohmic}$ ) with cycle number that can be explained by a continuous electrolyte decomposition associated with the growth of SEI and/or CEI layers. However, the major impedance growth was observed from the interfacial impedance of the full-cells. The total polarization resistances of the full-cells are plotted in Figure 2e. The baseline electrolyte gains the impedance rapidly during the first 50 cycles, followed by a steady growth to the 200th cycle. The 1 wt % TEB maintained the lowest impedance values at all cycles. However, further increase in TEB content to ≥3 wt % lead to a rapid impedance growth mainly at interfaces (Table S1). This result implies that excess amount of TEB would lead to their continuous reactions at electrode-electrolyte interfaces and thicken the interfacial layers. Considering their modest capacity retention behaviors (see Figure 1b), it is apparent that such interfacial reaction would not involve unwanted active Liion consumptions. Despite the unwanted increase in cell impedance, 4 wt % TEB still provided improved capacity

compared with the baseline cell. However, because the cell impedance growth leads to unwanted power loss in battery cells, it would not be recommended to add more than 2 wt % TEB in full-cells.

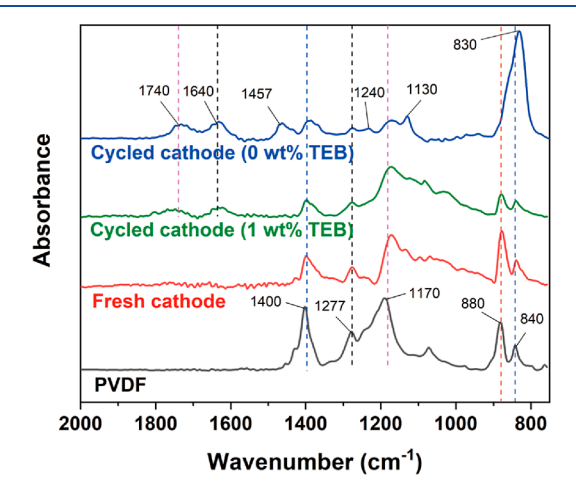
Understanding the Roles of TEB on Electrode–Electrolyte Interfaces in Full-Cells. Transition metal dissolution is known to be the major issue of the LNMO cathode in full-cells.  $^{12,13}$  The dissolved transition metals, particularly Mn, transport and damage the graphite SEI layer. In the literature, it was reported that TEB could suppress the Mn dissolution of LNMO and LiNi $_{1/3}$ Co $_{1/3}$ Mn $_{1/3}$ O $_2$  cathodes in half-cells.  $^{18,21}$  In our experiment, the amount of Mn deposition on cycle-aged graphite anode was measured by ICP–MS. Table 1 demonstrates a trend of decreasing Mn deposition on graphite anode with TEB additive contents in the electrolytes, which agrees well with the earlier reports.  $^{18,21}$ 

Table 1. Mn Deposition Amounts on Cycle-Aged Graphite Anodes Depending on Different TEB Contents in the Electrolytes, Which Were Analyzed by ICP–MS<sup>a</sup>

	Mn contents (ppm)
baseline electrolyte	4651
1 wt % TEB	4235
2 wt % TEB	4091
3 wt % TEB	3976
4 wt % TEB	3773

<sup>a</sup>The graphite anodes were recovered from LNMO/graphite full-cells after 200 cycles at 25 °C.

Because the Mn dissolution behavior originates from the parasitic reactions at CEI, we characterized the surface of cycled LNMO cathode by FTIR spectrometry. Figure 3 compares



**Figure 3.** FTIR spectra of fresh and 200-times cycled LNMO cathodes that were recovered from full-cells having the baseline (0 wt % TEB) and 1 wt % TEB additive in the electrolyte. PVdF binder spectrum was included for a reference.

FTIR spectra of fresh and cycled LNMO cathodes. Here, the peaks at 1400, 1277, 1170, 880, and 840 cm<sup>-1</sup> are attributed to the PVdF binder. <sup>17</sup> For the cycled cathode using the baseline electrolyte, its spectrum has some extra peaks appearing at 830 cm<sup>-1</sup>, which corresponds to P–F produced by a decomposition of LiPF<sub>6</sub> during the cycling. <sup>26</sup> The peaks at around 1740 and 1240 cm<sup>-1</sup> are characteristic of polyethylene carbonate (C<sub>2</sub>H<sub>4</sub>CO<sub>3</sub>)<sub>n</sub> product from the EC oxidation. <sup>27</sup> Also, the peak

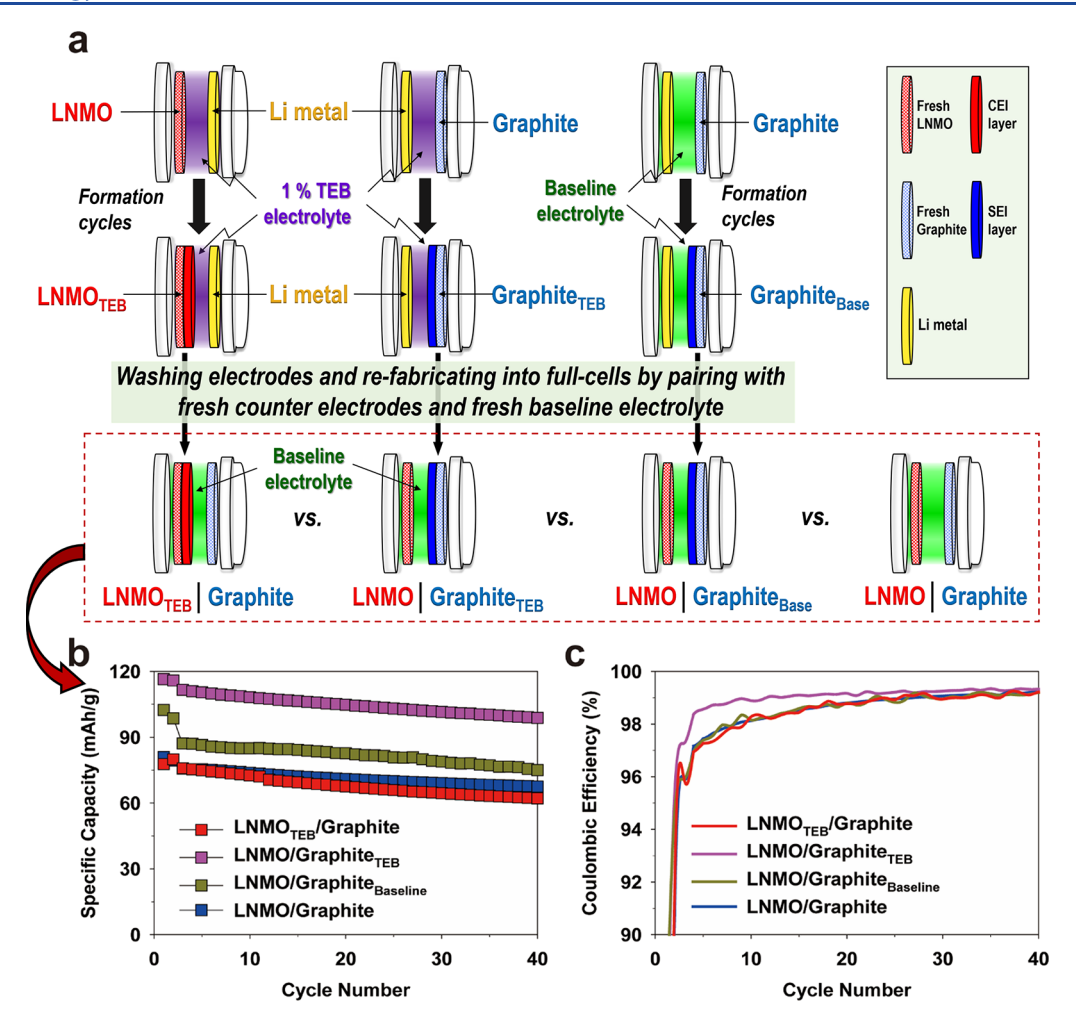


Figure 4. (a) Schematic diagram illustrating the combinatorial testing procedure designed for examining the effect of TEB-treated CEI at LNMO cathode and SEI at graphite anode on full-cell performances. (b) Cycle-life and (c) Coulombic efficiency of full-cells prepared by the different combinations of cathode and anode with and without TEB treatment (i.e., cycling with TEB additive in half-cells before full-cell fabrication), as illustrated in Figure 4a. Here, TEB-treated electrodes are denoted by LNMO<sub>TEB</sub> and graphite<sub>TEB</sub>. Further, graphite cycled in half-cell before the full-cell fabrication is denoted by graphite<sub>Baseline</sub> or graphite<sub>Base</sub>. First two cycles of the full-cells were performed at C/10 rate, followed by C/3 rate cycling during the remaining cycles.

at around 1640 cm<sup>-1</sup> is reported to be alkyl carbonate salt ROCO<sub>2</sub>-M<sup>n+</sup> and/or carboxylate salt RCO<sub>2</sub>-M<sup>n+</sup> (M = Li/Ni/Mn), the 1457 cm<sup>-1</sup> peak belongs to symmetric stretching of CO<sub>3</sub> in Li<sub>2</sub>CO<sub>3</sub>, and the 1130 cm<sup>-1</sup> peak belongs to the C–0. Compared with the cycled cathode in the baseline electrolyte (0 wt % TEB), the cycled cathode using 1 wt % TEB additive in the electrolyte delivered negligible intensities for the P–F peak at 830 cm<sup>-1</sup> and CO<sub>3</sub> peak at 1457 cm<sup>-1</sup>. Also, it has reduced intensities of 1130, 1640, and 1740 cm<sup>-1</sup> peaks. Overall, the FTIR data confirms that the 1 wt % TEB additive can suppress the parasitic reactions occurring at CEI after the extended cycling (i.e., 200 cycles).

In order to understand the improvement mechanism of TEB on the LNMO/graphite full-cell performances, we designed the experiments illustrated in Figure 4a. LNMO/Li and graphite/Li half-cells with 1 wt % TEB added electrolyte underwent formation cycles (3 cycles) at 0.1 C at 25 °C. The cycled electrodes were recovered from half-cells, followed by gently washing with baseline electrolyte for 20 min to remove residual TEB. Hereafter, these aged electrodes that underwent the formation cycles using the TEB additive are denoted by LNMO<sub>TEB</sub> and graphite<sub>TEB</sub>. The LNMO<sub>TEB</sub> and graphite<sub>TEB</sub>

were, respectively, paired with fresh graphite and LNMO to refabricate into full-cells using the baseline (i.e., TEB-free) electrolyte.

Figure 4b,c compares the cycle life and Coulombic efficiency (CE) of the full-cells prepared by the various electrode combinations listed in Figure 4a. First, the LNMO<sub>TEB</sub>/graphite delivered the initial specific capacity and the CE values that were similar to those of the non-treated LNMO/graphite cell (i.e., no prior TEB treatment). At the 50th cycle, the LNMO<sub>TEB</sub>/ graphite cell delivered slightly lower capacity than that of the LNMO/graphite cell. Even after considering a slight damage of the LNMO<sub>TEB</sub> electrode during its recovery from the cycled cell and refabrication into a full-cell, its lack of immediate performance improvement in the full-cell with identical CE and initial capacity may indicate that CEI at the LNMO electrode would not offer a benefit during the SEI formation on graphite anodes. Because the Mn dissolution could be a slow process occurring during long-term cycling, the TEB-treated CEI on LNMO<sub>TEB</sub> would not deliver improved performance at an early stage of cycling. For example, it should be reminded that the Mn-dissolution amounts on graphite SEIs in Table 1 were determined after 200 cycles.

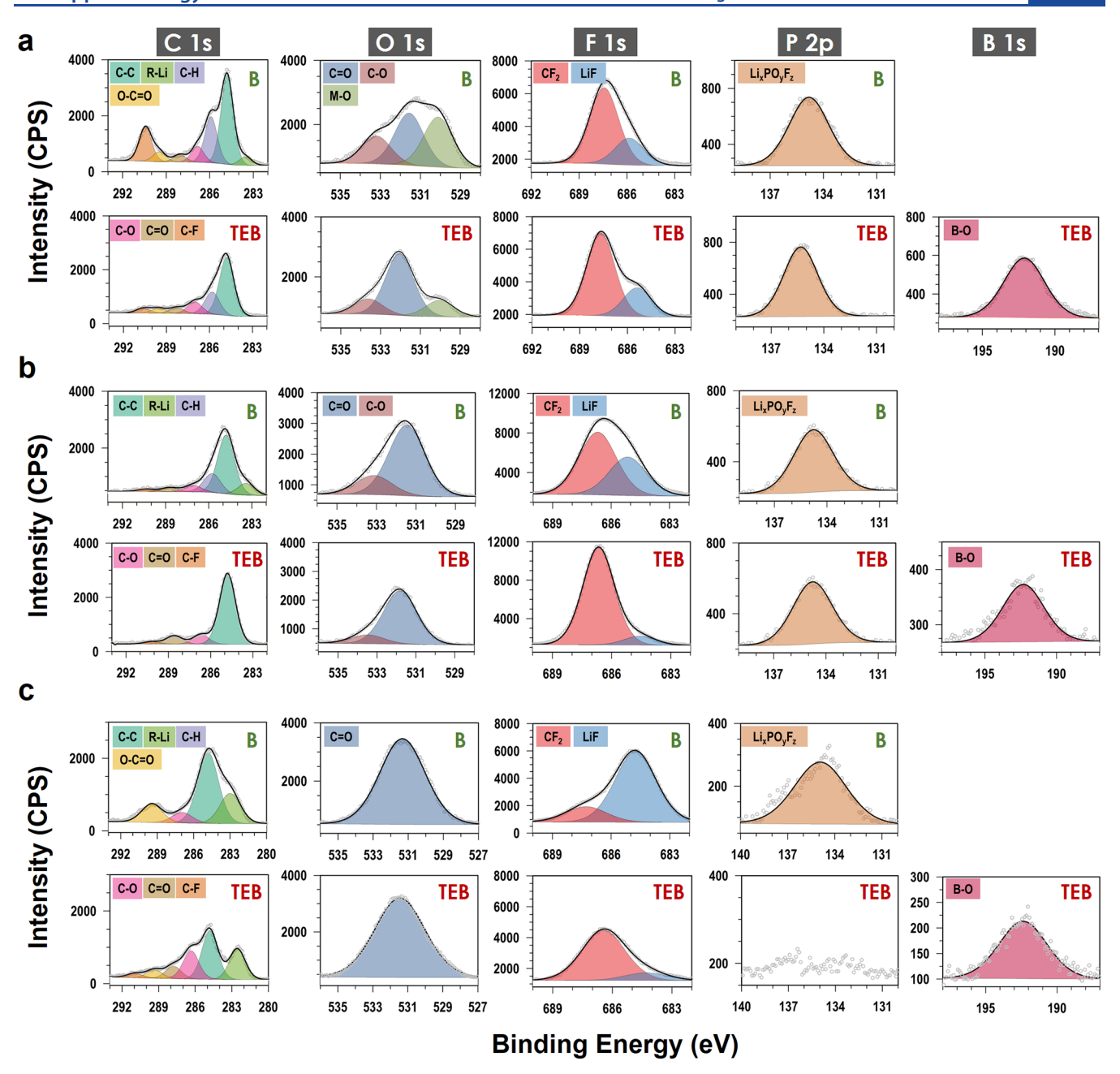


Figure 5. XPS spectra comparing the effect of (i) baseline (marked with "B") and (ii) 1 wt % TEB additive (marked with "TEB") electrolyte on the (a) CEI in LNMO cathodes after 200 cycles; (b) SEI at graphite anodes after 200 cycles; and (c) SEI at graphite anodes after the 1st cycle in full-cells. XPS spectra were taken at the elemental regions of C 1s, O 1s, F 1s, P 2p, and B 1s. The gray circles represent the experimental data, and the solid black line represents the fitted curve.

In contrast, the LNMO/graphite<sub>TEB</sub> delivered a high initial capacity of 117 mA h/g at C/10 rate and 112 mA h/g at C/3 rate. Because the graphite anode in the LNMO/graphite<sub>TEB</sub> cell had a pre-formed SEI layer from previous half-cell cycling, its high capacity can be partly explained by reducing irreversible Liion consumptions that are necessary during the SEI formation. Therefore, to make a reasonable comparison, we also prepared the cycled graphite (denoted by graphite<sub>Base</sub>) in half-cell using the TEB-free, baseline electrolyte and paired it with a fresh cathode to fabricate into a full-cell using the baseline electrolyte (LNMO/graphite<sub>Base</sub>), as illustrated in Figure 4a. The resulting full-cell data shows some capacity improvement compared to the LNMO/graphite cell, as shown in Figure 4b. However, the specific capacity and the CE of the LNMO/graphite<sub>Base</sub> are

inferior to those of the LNMO/graphite  $_{TEB}$ . This result confirms that TEB-produced graphite SEI (i.e., graphite  $_{TEB}$ ) delivers more effective passivation on the anode than that of the standard SEI (i.e., graphite  $_{Base}$ ) produced by the baseline electrolyte on the anode.

XPS analysis was conducted further to identify chemical species of CEI and SEI layers, respectively, on cycle-aged cathodes and anodes after recovering from the 200 times cycled full-cells. Figure 5a shows XPS spectra of LNMO cathodes cycled in the baseline and 1 wt % TEB electrolyte. For the LNMO cathode cycled in the baseline electrolyte, the C–C bond at  $\sim$ 284.8 eV is mainly from conductive carbon agent, while the C–O ( $\sim$ 286.8 eV), C=O ( $\sim$ 288.2 eV), and O–C=O ( $\sim$ 289.4 eV) bonds are mainly derived from CEI layer

products including  $(C_2H_4CO_3)_n$ ,  $ROCO_2Li$ ,  $RCO_2Li$ ,  $LiCO_3$ , and ROLi,  $^{30-33}$  which was also observed from the FTIR data. The C-F bond is from the PVdF binder. In the O 1s spectrum of the cathode in the baseline electrolyte, the signals at 530, 531.8, and 533.4 eV can be assigned to Me-O (metal oxide from LNMO), C=O, and C-O, respectively. Its F 1s spectrum mainly comprises PVdF peak at 687.6 eV and LiF peak at 685.6 eV. The LiF can be produced via the decomposition of LiPF<sub>6</sub> into LiF and PF<sub>5</sub>. The peak appearing at ~135 eV from its P 2p spectrum can be assigned to  $\text{Li}_x PO_y F_y$  which is an electrolyte decomposition product of high-voltage cathodes.

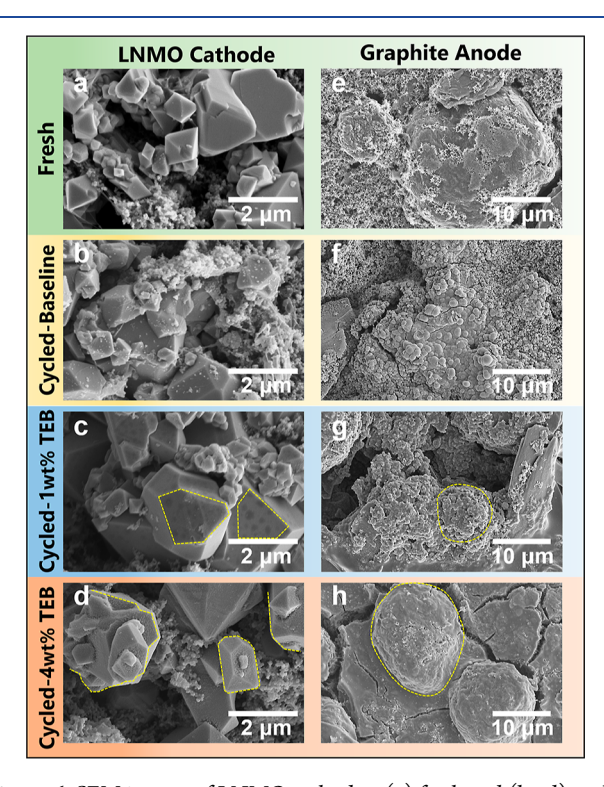
For LNMO cathode cycled in 1 wt % TEB electrolyte, the peak at ~192 eV in B 1s spectrum belongs to B–O, which proves the participation of TEB in the CEI formation. 1 Its C 1s spectrum did not contain the peak corresponding to the RLi. The PVdF binder peak (C–F bond ~290.4 eV) and Me–O peak (~530 eV) intensities were relatively lower than that of the baseline electrolyte, suggesting that the TEB additive led to a formation of thicker CEI after 200 cycles. The O 1s, F 1s, and P 2p spectra from the 1 wt % TEB additive showed similar CEI components compared with the CEI from the baseline electrolyte.

Figure 5b compares XPS spectra of 200-times-cycled graphite anodes using the baseline and 1 wt % TEB-added electrolytes. As observed from the CEI, XPS spectra show the presence of the B peak at ~192 eV and confirm the contribution of TEB on the formation of the graphite SEI.<sup>21</sup> Compared with the baseline electrolyte, 1 wt % TEB additive suppressed the formation of R-Li at 283.4 eV and C-H at 285.8 eV, parts of the electrolyte decomposition products. The most remarkable difference was found from the LiF peaks in F 1s spectra; LiF intensity from TEB containing anode is much less than that from the baseline electrolyte. Considering that LiF is the end product of various decomposition reactions from electrolyte solvents (e.g., EC, DEC), a salt (e.g., LiPF<sub>6</sub>), and other SEI components (e.g., Li<sub>2</sub>CO<sub>3</sub> and Li<sub>2</sub>O), <sup>36</sup> this result suggests that TEB additive can mitigate the electrolyte decomposition occurring at the graphite SEI.37

It is noticeable that the effect of TEB additive on the full-cell was immediately observed from the 1st cycle capacity: for example, 82 mA h/g for baseline electrolyte and 110 mA h/g for 1 wt % TEB electrolyte. This result suggests that the Li<sup>+</sup> loss during the formation of SEI on graphite was effectively mitigated by employing the TEB additive. Therefore, we further characterized the graphite SEI after the 1st cycle in LNMO/ graphite full-cells prepared using the (i) baseline electrolyte and (ii) 1 wt % TEB electrolyte. Figure 5c compares their resulting XPS spectra at the core level of various elemental regions. In the C 1s region, C-F peak from the PVdF binder is noticeable from the graphite SEI with 1 wt % TEB but is difficult to detect from the baseline electrolyte. This trend is confirmed from the F 1s region, where PVdF peak intensity was much stronger from the 1 wt % TEB electrolyte than the baseline electrolyte. The B-O peak is clearly observed in the B 1s region, indicating that TEB participates in the initial SEI formation on graphite. More importantly, LiF (F 1s region) and Li<sub>x</sub>PO<sub>y</sub>F<sub>z</sub> (P 2p region) species shown from the baseline electrolyte are negligible from the 1 wt % TEB additive. These results coherently corroborate that TEB additive contributes to the thinner SEI layer formation by reducing the EC decomposition during the 1st charging process (i.e., the formation cycle). As a result, the 1 wt % TEB additive reduced the amount of Li<sup>+</sup> consumption during the initial SEI formation and consequently retained higher initial

capacity (110 mA h/g) than that of the baseline electrolyte (82 mA h/g).

Figure 6a-d compares SEM images of the pristine and 200times-cycled LNMO cathodes, which were recovered from the



**Figure 6.** SEM images of LNMO cathodes: (a) fresh and (b-d) cycleaged cathodes collected from full-cells after cycling 200 times using the (b) baseline electrolyte, (c) 1 wt % TEB, and (d) 4 wt % TEB additives, respectively. SEM images of graphite anodes: (e) fresh graphite anode and (f-h) cycle-aged anodes collected from full-cells after cycling 200 times using the (f) baseline electrolyte, (g) 1 wt % TEB, and (h) 4 wt % TEB additive, respectively. The characteristic CEI and SEI morphology formed by TEB is highlighted in yellow. Additional SEM images are shown in Figure S3.

full-cells with the baseline and 1 and 4 wt % TEB-added electrolytes. The pristine cathode, as shown in Figures 6a and S3a, consists of micron-sized LNMO particles and nano-sized carbon black particles. After cycling in the baseline electrolyte, the electrode surface is covered with some deposited materials, as shown in Figures 6b and S3b, which would be produced by the parasitic reactions at CEI at high voltages, as reported in the literature. 12 For the cathode cycled in 1 wt % TEB, Figures 6c and S3c reveal some coated areas shown as dark spots on LNMO particle surfaces, indicating the different CEI morphologies produced by the TEB additive as evidenced by the XPS analysis. For the cathode cycled in 4 wt % TEB, as shown in Figures 6d and S3d, most of the LNMO particle surfaces were evenly coated with films that were clearly visible compared with other cycleaged samples. This thick CEI would be responsible for the large  $R_{\text{int}}$  values as shown in Figure 2d. The SEM data shows TEB's contributes to the formation and growth of CEI layer during the cycling, in good agreement with literature. 19,20

Figure 6e—h compares SEM images of pristine and 200-times-cycled graphite anodes with the baseline and 1 and 4 wt % TEB-added electrolytes, which were paired with the same cathodes shown in Figure 6a—d. Figures 6e and S3e show the pristine anode consisting of spherical MCMB graphite having sizes in a

range of  $10-25~\mu m$  and nano-sized carbon. After 200 cycles in the baseline electrolyte, Figures 6f and S3f show a thick SEI layer covering most of the surface of the anode. The micro-cracks at the surface of SEI can be produced while drying the electrode that accompanies significant volumetric changes of the SEI layer. Due to the dense and thick SEI layer, the morphology of the graphite underneath the SEI could not be observable. The SEI produced by the baseline electrolyte has granular morphologies covering the whole graphite anodes. <sup>41</sup>

In contrast, the morphology of cycled anode in 1 wt % TEB shows less decomposition product in Figures 6g and S3g, while it occasionally shows a smooth and film-like SEI morphology. The increase in TEB content from 1 to 4 wt % led to the coverage of the whole graphite particles with the smooth SEI film as shown in Figures 6h and S3h. For example, individual graphite particles underneath the SEI layer are discernible across the anode surfaces. This result suggests that TEB additive offers a controlled way of the SEI layer growth and thus maintains a limited SEI thickness during the extended period of battery cycling, in comparison to the SEI produced by the baseline electrolyte. Overall, the 1 wt % TEB additive can effectively improve the stability of graphite SEI and lead to the significant performance improvement of LNMO/graphite full-cells in terms of energy and power density.

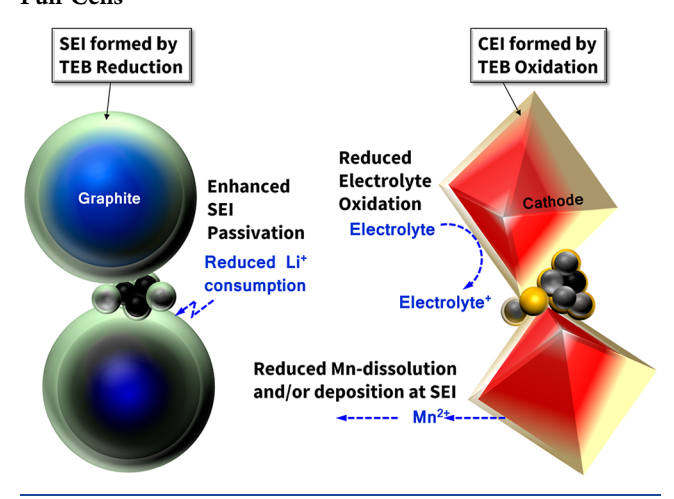
The surface characterization data clearly demonstrated that TEB contributed to the formation of both CEI and SEI layers. For CEI, the participation of TEB could suppress the parasitic reaction and reduce the Mn dissolution after 200 cycles (see, Table 1). At the same time, high TEB contents (>3 wt %) led to a thicker CEI layer and large interfacial impedance (see Figure 2). Liu et al. 42 reported the formation process of cathode CEI involving trimethyl borate (TMB) and tripropyl borate (TPB) additives, which have a molecular structure similar to that of TEB (all contain borate esters). Their systematic calculations showed that the B-O and C-O bond lengths became longer after one-electron oxidation, suggesting that B-O and C-O bonds would be broken, and the resulting species combined with HF and dehydrogenated EC to participate in the construction of the interphase. 42 For the SEI, TEB-treated graphite<sub>TEB</sub> showed immediate performance improvement (see Figure 4) due to the improved SEI stability and reduced Li-ion loss, as evidenced by XPS data (i.e., reduced LiF contents in Figure 5c). Li et al.<sup>43</sup> reported that B-O bonds in 2,4,6-triphenyl boroxine (TPBX) were broken after one-electron reduction and subsequently initiated polymerization reaction on SEI layer. From the similarity of B-O networking, the results can explain how TEB contributes to the formation of graphite SEI. In this work, we focused on the impact of TEB on interfacial stability and performance of LNMO/graphite full-cells, to fill the knowledge gap in the literature. Future research will be focused on the chemical reaction mechanism in both CEI and SEI, assisted by experimental and computational calculations.

#### CONCLUSIONS

The role of TEB electrolyte additive on the interfacial stabilities of electrodes in high-voltage spinel cathode and graphite anode in LIBs was systematically investigated. Electrochemical characterization data presented that TEB additive improved full-cell capacity and lowered the cell impedances during the extended period of cycling. We characterized the effect of TEB additive in 0–4 wt % contents on CEI and SEI of LNMO/graphite full-cells. Increasing TEB contents in electrolyte reduced the Mn dissolution and deposition at graphite anodes

(Table 1). However, a combinatorial study of the TEB-treated graphite and TEB-treated LNMO electrodes (Figure 4) and XPS analysis (Figure 6) revealed that the short-term performance improvement shown by the full-cells (see Figure 1b) was mostly contributed by the improved SEI stability on graphite anodes and mitigating the Li<sup>+</sup> loss (i.e., production of LiF in SEI). Because the Mn dissolution is a slow but continuous process occurring during an extended cycling, LNMO<sub>TEB</sub> may not deliver an improved performance at the early stage of cycling. Among the various TEB contents (0-4 wt %) investigated, 1 wt % TEB offered combined advantages of high capacity and low cell impedance due to the stabilized CEI and SEI. At the same time, TEB-added full-cells still showed a nonnegligible amount of Mn deposition on graphite SEI, suggesting that the TEB additive alone would not perfectly passivate CEI and SEI layers during the high-voltage (e.g., up to 4.9 V vs Li) operation. Although literature data mostly focused on the impacts of TEB on CEI in half-cell configurations, our full-cell analyses revealed an additional benefit of TEB-significant improvement of graphite SEI stability. Finally, Scheme 1

Scheme 1. Multiple Roles of TEB Additive in CEI at LNMO Cathode and SEI at Graphite Anode in LNMO/Graphite Full-Cells



illustrates the multiple roles of the TEB additive in the fullcells. Based on the result, TEB is expected to offer promising performance improvements in various types of high-voltage LIBs.

#### ASSOCIATED CONTENT

#### Supporting Information

The Supporting Information is available free of charge at https://pubs.acs.org/doi/10.1021/acsaem.2c00861.

EIS fitting data deconvoluting each impedance sources of full-cells during cycling; voltage and  $\mathrm{d}Q/\mathrm{d}V$  profiles of half-cells; and additional SEM images of cycled LNMO and graphite electrodes (PDF)

### AUTHOR INFORMATION

## **Corresponding Author**

Jung-Hyun Kim — Center for Automotive Research, Department of Mechanical and Aerospace Engineering, The Ohio State University, Columbus, Ohio 43212, United States;

orcid.org/0000-0002-4598-4686; **Email**: kim.6776@osu.edu

#### **Authors**

- Tianyang Wang Center for Automotive Research, Department of Mechanical and Aerospace Engineering, The Ohio State University, Columbus, Ohio 43212, United States
- Lalith Rao Center for Automotive Research, Department of Mechanical and Aerospace Engineering, The Ohio State University, Columbus, Ohio 43212, United States
- Xinwei Jiao Center for Automotive Research, Department of Mechanical and Aerospace Engineering, The Ohio State University, Columbus, Ohio 43212, United States
- Junbin Choi Center for Automotive Research, Department of Mechanical and Aerospace Engineering, The Ohio State University, Columbus, Ohio 43212, United States
- Junwei Yap Center for Automotive Research, Department of Mechanical and Aerospace Engineering, The Ohio State University, Columbus, Ohio 43212, United States

Complete contact information is available at: https://pubs.acs.org/10.1021/acsaem.2c00861

#### Notes

The authors declare no competing financial interest.

#### ACKNOWLEDGMENTS

This research was financially sponsored by the U.S. Department of Energy's Office of Energy Efficiency & Renewable Energy (EERE) project "Cobalt-Free Cathodes for Next-Generation Lithium-Ion Batteries" under contract no. DE-EE0008446. Characterization of this work was supported in part by the Ohio State University Institute for Materials Research.

#### REFERENCES

- (1) Tarascon, J.-M.; Armand, M. Issues and Challenges Facing Rechargeable Lithium Batteries. *Nature* **2001**, *414*, 359–367.
- (2) Shi, C.; Wang, T.; Liao, X.; Qie, B.; Yang, P.; Chen, M.; Wang, X.; Srinivasan, A.; Cheng, Q.; Ye, Q.; Li, A. C.; Chen, X.; Yang, Y. Accordion-like Stretchable Li-Ion Batteries with High Energy Density. *Energy Storage Mater.* **2019**, *17*, 136–142.
- (3) Lu, L.; Han, X.; Li, J.; Hua, J.; Ouyang, M. A Review on the Key Issues for Lithium-Ion Battery Management in Electric Vehicles. *J. Power Sources* **2013**, 226, 272–288.
- (4) Patoux, S.; Daniel, L.; Bourbon, C.; Lignier, H.; Pagano, C.; Le Cras, F.; Jouanneau, S.; Martinet, S. High Voltage Spinel Oxides for Li-Ion Batteries: From the Material Research to the Application. *J. Power Sources* **2009**, *189*, 344–352.
- (5) Julien, C. M.; Mauger, A. Review of 5-V Electrodes for Li-Ion Batteries: Status and Trends. *Ionics* **2013**, *19*, 951–988.
- (6) Zhong, Q.; Bonakdarpour, A.; Zhang, M.; Gao, Y.; Dahn, J. R. Synthesis and Electrochemistry of LiNi  $\times$  Mn<sub>2</sub>  $\times$ O<sub>4</sub>. *J. Electrochem. Soc.* **1997**, *144*, 205–213.
- (7) Kim, J.-H.; Pieczonka, N. P. W.; Yang, L. Challenges and Approaches for High-Voltage Spinel Lithium-Ion Batteries. *Chem-PhysChem* **2014**, *15*, 1940–1954.
- (8) Goodenough, J. B.; Kim, Y. Challenges for Rechargeable Li Batteries. *Chem. Mater.* **2010**, 22, 587–603.
- (9) Xu, K. Nonaqueous Liquid Electrolytes for Lithium-Based Rechargeable Batteries. *Chem. Rev.* **2004**, *104*, 4303–4418.
- (10) Yang, L.; Ravdel, B.; Lucht, B. L. Electrolyte Reactions with the Surface of High Voltage LiNi<sub>0.5</sub>Mn<sub>1.5</sub>O<sub>4</sub> Cathodes for Lithium-Ion Batteries. *Electrochem. Solid-State Lett.* **2010**, *13*, A95–A97.
- (11) Xu, K. Electrolytes and Interphases in Li-Ion Batteries and Beyond. Chem. Rev. 2014, 114, 11503-11618.
- (12) Pieczonka, N. P. W.; Liu, Z.; Lu, P.; Olson, K. L.; Moote, J.; Powell, B. R.; Kim, J.-H. Understanding Transition-Metal Dissolution Behavior in LiNio. 5Mn1. 5O4 High-Voltage Spinel for Lithium Ion Batteries. *J. Phys. Chem. C* 2013, 117, 15947–15957.

- (13) Kim, J.-H.; Pieczonka, N. P. W.; Li, Z.; Wu, Y.; Harris, S.; Powell, B. R. Understanding the Capacity Fading Mechanism in LiNi0.5M-n1.5O4/Graphite Li-Ion Batteries. *Electrochim. Acta* **2013**, *90*, 556–562.
- (14) Burns, J. C.; Petibon, R.; Nelson, K. J.; Sinha, N. N.; Kassam, A.; Way, B. M.; Dahn, J. R. Studies of the Effect of Varying Vinylene Carbonate (VC) Content in Lithium Ion Cells on Cycling Performance and Cell Impedance. *J. Electrochem. Soc.* **2013**, *160*, A1668—A1674.
- (15) Abe, K.; Ushigoe, Y.; Yoshitake, H.; Yoshio, M. Functional Electrolytes: Novel Type Additives for Cathode Materials, Providing High Cycleability Performance. *J. Power Sources* **2006**, *153*, 328–335.
- (16) Birrozzi, A.; Laszczynski, N.; Hekmatfar, M.; von Zamory, J.; Giffin, G. A.; Passerini, S. Beneficial Effect of Propane Sultone and Tris(Trimethylsilyl) Borate as Electrolyte Additives on the Cycling Stability of the Lithium Rich Nickel Manganese Cobalt (NMC) Oxide. *J. Power Sources* **2016**, 325, 525–533.
- (17) Pieczonka, N. P. W.; Yang, L.; Balogh, M. P.; Powell, B. R.; Chemelewski, K.; Manthiram, A.; Krachkovskiy, S. A.; Goward, G. R.; Liu, M.; Kim, J.-H. Impact of Lithium Bis(Oxalate)Borate Electrolyte Additive on the Performance of High-Voltage Spinel/Graphite Li-Ion Batteries. *J. Phys. Chem. C* 2013, 117, 22603–22612.
- (18) Wang, Z.; Xing, L.; Li, J.; Xu, M.; Li, W. Triethylborate as an Electrolyte Additive for High Voltage Layered Lithium Nickel Cobalt Manganese Oxide Cathode of Lithium Ion Battery. *J. Power Sources* **2016**, 307, 587–592.
- (19) Liu, Q.; Yang, G.; Liu, S.; Han, M.; Wang, Z.; Chen, L. Trimethyl Borate as Film-Forming Electrolyte Additive To Improve High-Voltage Performances. *ACS Appl. Mater. Interfaces* **2019**, *11*, 17435–17443.
- (20) Li, J.; Wang, Z. Triethyl Borate and Tripropyl Borate as Electrolyte Additives for 4.8 V High Voltage Layered Lithium-Rich Oxide Cathode with Enhanced Self-Discharge Suppression Performance: A Comparative Study. *J. Power Sources* **2020**, 450, 227648.
- (21) Chen, Z.; Wang, C.; Xing, L.; Wang, X.; Tu, W.; Zhu, Y.; Li, W. Borate Electrolyte Additives for High Voltage Lithium Nickel Manganese Oxide Electrode: A Comparative Study. *Electrochim. Acta* **2017**, 249, 353–359.
- (22) Li, J.; Zhang, L.; Yu, L.; Fan, W.; Wang, Z.; Yang, X.; Lin, Y.; Xing, L.; Xu, M.; Li, W. Understanding Interfacial Properties between Li-Rich Layered Oxide and Electrolyte Containing Triethyl Borate. *J. Phys. Chem. C* 2016, 120, 26899–26907.
- (23) Xu, S.-D.; Zhuang, Q.-C.; Tian, L.-L.; Qin, Y.-P.; Fang, L.; Sun, S.-G. Impedance Spectra of Nonhomogeneous, Multilayered Porous Composite Graphite Electrodes for Li-Ion Batteries: Experimental and Theoretical Studies. *J. Phys. Chem. C* **2011**, *115*, 9210–9219.
- (24) Xu, S.-D.; Zhuang, Q.-C.; Wang, J.; Xu, Y.-Q.; Zhu, Y.-B. New Insight into Vinylethylene Carbonate as a Film Forming Additive to Ethylene Carbonate-Based Electrolytes for Lithium-Ion Batteries. *Int. J. Electrochem. Sci.* **2013**, *8*, 8058–8076.
- (25) Schmidt, J. P.; Chrobak, T.; Ender, M.; Illig, J.; Klotz, D.; Ivers-Tiffée, E. Studies on LiFePO4 as Cathode Material Using Impedance Spectroscopy. *J. Power Sources* **2011**, *196*, 5342–5348.
- (26) Aurbach, D.; Weissman, I.; Zaban, A.; Chusid, O. Correlation between Surface Chemistry, Morphology, Cycling Efficiency and Interfacial Properties of Li Electrodes in Solutions Containing Different Li Salts. *Electrochim. Acta* 1994, 39, 51–71.
- (27) Dalavi, S.; Xu, M.; Knight, B.; Lucht, B. L. Effect of Added LiBOB on High Voltage (LiNi0.5Mn1.5O4) Spinel Cathodes. *Electrochem. Solid State Lett.* **2011**, *15*, A28–A31.
- (28) Lee, Y.-M.; Nam, K.-M.; Hwang, E.-H.; Kwon, Y.-G.; Kang, D.-H.; Kim, S.-S.; Song, S.-W. Interfacial Origin of Performance Improvement and Fade for 4.6 V LiNi<sub>0.5</sub>Co<sub>0.2</sub>Mn<sub>0.3</sub>O<sub>2</sub> Battery Cathodes. *J. Phys. Chem. C* **2014**, *118*, 10631–10639.
- (29) Marom, R.; Haik, O.; Aurbach, D.; Halalay, I. C. Revisiting LiClO<sub>4</sub> as an Electrolyte for Rechargeable Lithium-Ion Batteries. *J. Electrochem. Soc.* **2010**, *157*, A972.
- (30) Quinlan, R. A.; Lu, Y.-C.; Shao-Horn, Y.; Mansour, A. N. XPS Studies of Surface Chemistry Changes of LiNi<sub>0.5</sub>Mn<sub>0.5</sub>O<sub>2</sub> Electrodes during High-Voltage Cycling. *J. Electrochem. Soc.* **2013**, *160*, A669–A677.

- (31) Xu, M.; Hao, L.; Liu, Y.; Li, W.; Xing, L.; Li, B. Experimental and Theoretical Investigations of Dimethylacetamide (DMAc) as Electrolyte Stabilizing Additive for Lithium Ion Batteries. *J. Phys. Chem. C* **2011**, *115*, 6085–6094.
- (32) Martha, S. K.; Nanda, J.; Veith, G. M.; Dudney, N. J. Surface Studies of High Voltage Lithium Rich Composition: Li1.2Mn0.525-Ni0.175Co0.1O2. *J. Power Sources* **2012**, 216, 179–186.
- (33) Yang, L.; Markmaitree, T.; Lucht, B. L. Inorganic Additives for Passivation of High Voltage Cathode Materials. *J. Power Sources* **2011**, 196, 2251–2254.
- (34) Xiao, Z.-X.; Cui, S.-L.; Wang, Y.-Y.; Liu, S.; Li, G.-R.; Gao, X.-P. Enabling LiNi $_{0.88}$ Co $_{0.09}$ Al $_{0.03}$ O $_{2}$  Cathode Materials with Stable Interface by Modifying Electrolyte with Trimethyl Borate. *ACS Sustainable Chem. Eng.* **2021**, *9*, 1958–1968.
- (35) Yang, X.; Li, J.; Xing, L.; Liao, Y.; Xu, M.; Huang, Q.; Li, W. Stabilizing Lithium Manganese Oxide/Organic Carbonate Electrolyte Interface with a Simple Boron-Containing Additive. *Electrochim. Acta* 2017, 227, 24–32.
- (36) An, S. J.; Li, J.; Daniel, C.; Mohanty, D.; Nagpure, S.; Wood, D. L. The State of Understanding of the Lithium-Ion-Battery Graphite Solid Electrolyte Interphase (SEI) and Its Relationship to Formation Cycling. *Carbon* **2016**, *105*, 52–76.
- (37) Wang, K.; Xing, L.; Zhi, H.; Cai, Y.; Yan, Z.; Cai, D.; Zhou, H.; Li, W. High Stability Graphite/Electrolyte Interface Created by a Novel Electrolyte Additive: A Theoretical and Experimental Study. *Electrochim. Acta* 2018, 262, 226–232.
- (38) Madec, L.; Xia, J.; Petibon, R.; Nelson, K. J.; Sun, J.-P.; Hill, I. G.; Dahn, J. R. Effect of Sulfate Electrolyte Additives on LiNi1/3Mn1/3Co1/3O2/Graphite Pouch Cell Lifetime: Correlation between XPS Surface Studies and Electrochemical Test Results. *J. Phys. Chem. C* 2014, 118, 29608–29622.
- (39) Klein, S.; Harte, P.; Henschel, J.; Bärmann, P.; Borzutzki, K.; Beuse, T.; Wickeren, S.; Heidrich, B.; Kasnatscheew, J.; Nowak, S.; Winter, M.; Placke, T. On the Beneficial Impact of Li <sub>2</sub> CO <sub>3</sub> as Electrolyte Additive in NCM523 || Graphite Lithium Ion Cells Under High-Voltage Conditions. *Adv. Energy Mater.* **2021**, *11*, 2003756.
- (40) Zuo, X.; Fan, C.; Xiao, X.; Liu, J.; Nan, J. High-Voltage Performance of LiCoO2/Graphite Batteries with Methylene Methanedisulfonate as Electrolyte Additive. *J. Power Sources* **2012**, *219*, 94–99.
- (41) Zhang, P.; Yuan, T.; Pang, Y.; Peng, C.; Yang, J.; Ma, Z.-F.; Zheng, S. Influence of Current Density on Graphite Anode Failure in Lithium-Ion Batteries. *J. Electrochem. Soc.* **2019**, *166*, A5489—A5495.
- (42) Li, J.; Liao, Y.; Fan, W.; Li, Z.; Li, G.; Zhang, Q.; Xing, L.; Xu, M.; Li, W. Significance of Electrolyte Additive Molecule Structure in Constructing Robust Interphases on High-Voltage Cathodes. ACS Appl. Energy Mater. 2020, 3, 3049–3058.
- (43) Li, G.; Liao, Y.; Li, Z.; Xu, N.; Lu, Y.; Lan, G.; Sun, G.; Li, W. Constructing a Low-Impedance Interface on a High-Voltage LiNi<sub>0.8</sub>Co<sub>0.1</sub>Mn<sub>0.1</sub>O<sub>2</sub> Cathode with 2,4,6-Triphenyl Boroxine as a Film-Forming Electrolyte Additive for Li-Ion Batteries. *ACS Appl. Mater. Interfaces* **2020**, *12*, 37013–37026.

# ☐ Recommended by ACS

Enhanced Electrochemical Performance of the  $LiNi_{0.5}Mn_{1.5}O_4$  Cathode Material by the Construction of Uniform Lithium Silicate Nanoshells

Yuan Zhang, Guangchuan Liang, et al.

DECEMBER 23, 2022

ACS APPLIED MATERIALS & INTERFACES

READ 🗹

Aqueous Processing of LiCoO<sub>2</sub>–Li<sub>6.6</sub>La<sub>3</sub>Zr<sub>1.6</sub>Ta<sub>0.4</sub>O<sub>12</sub> Composite Cathode for High-Capacity Solid-State Lithium Batteries

Ruijie Ye, Martin Finsterbusch, et al.

MARCH 21, 2023

ACS SUSTAINABLE CHEMISTRY & ENGINEERING

READ 🗹

Influence of Cobalt Introduction on the Phase Equilibrium and Sintering Behavior of Lithium-Ion Conductor Li<sub>1.3</sub>Al<sub>0.3</sub>Ti<sub>1.7</sub>(PO<sub>4</sub>)<sub>3</sub>

Shogo Miyoshi, Kazunori Takada, et al.

MAY 25, 2022

ACS APPLIED ENERGY MATERIALS

READ 🗹

Thermal Runaway Behavior of  $\text{Li}_6\text{PS}_5\text{Cl}$  Solid Electrolytes for  $\text{LiNi}_{0.8}\text{Co}_{0.1}\text{Mn}_{0.1}\text{O}_2$  and  $\text{LiFePO}_4$  in All-Solid-State Batteries

Taehun Kim, Kyu Tae Lee, et al.

OCTOBER 11, 2022

CHEMISTRY OF MATERIALS

READ 🗹

Get More Suggestions >